Thermal and Mechanical Design Considerations for INTOR

D.K. Sze, W.G. Homeyer, R.L. Creedon, C.P. Wong, and G.L. Kulcinski

October 1980

UWFDM-388

FUSION TECHNOLOGY INSTITUTE

UNIVERSITY OF WISCONSIN

MADISON WISCONSIN

Thermal and Mechanical Design Considerations for INTOR

D.K. Sze, W.G. Homeyer, R.L. Creedon, C.P. Wong, and G.L. Kulcinski

Fusion Technology Institute
University of Wisconsin
1500 Engineering Drive
Madison, WI 53706

http://fti.neep.wisc.edu

October 1980

UWFDM-388

Thermal and Mechanical Design Considerations for INTOR

D.K. Sze
W.G. Homeyer*
R.L. Creedon*
C.P. Wong*
G.L. Kulcinski

Fusion Engineering Program
Nuclear Engineering Department
University of Wisconsin
Madison WI 53706 U.S.A.

October 1980

UWFDM-388

*General Atomic Company, San Diego CA

1. SUMMARY OF MAJOR CONCLUSIONS

Two recommended designs have been developed for the divertor plates based on the input design conditions given in Table 1. The chief difference between these designs is the surface exposed to the plasma stream. In one design a solid armor material is used, while in the other design a renewable liquid film is used. Since each of these designs has certain advantages and uncertainties, it was not possible to select one. It is recommended that both be studied further.

1.1. RECOMMENDED DESIGN - COMMON FEATURES

Although the surfaces facing the plasma are quite different in the two designs, the designs have many features in common. These features are described in this section.

1.1.1. Contour of Divertor Plates

The poloidal divertor in INTOR would impose very high heat and particle loads on a target placed normal to the plasma stream. Such loads would make heat removal difficult and greatly limit the lifetime of the target due to erosion by charged particles and energetic neutrals. To reduce the heat and particle load on the divertor plates, they are inclined at an angle to the plasma stream.

It appears there is sufficient space for inclined divertor plates in the INTOR machine to allow the peak thermal load to be limited to 5 MW/m^2 (500 W/cm^2) and to allow the particle load to be limited to $10^{18} cm^{-2} s^{-1}$. This peak rate is still some 2½ times the average energy and particle load over the divertor plates for a double null divertor.

To limit the heat flux on the outer divertor plate to 5 MW/m^2 requires that the plate cross the separatrix at an angle less than

TABLE 1. SUMMARY OF INPUT DESIGN CONDITIONS

BASIC INPUT	
Energy to Outer Divertor Plate[a]	75 MW
Energy to Inner Divertor Plate[a]	25 MW
Total Particle Load	$2 \times 10^{23} s^{-1}$
Ion Energy	1.3 keV
Width of Divertor Ducts	30 cm
e-Folding Distance[b]	5 cm
D:T:He	0.475:0.475:0.05
Duty Cycle	0.7
Availability	0.25
DERIVED CONDITIONS	
Helium Pressure in Collector Chamber	2.2×10^{-5} torr
Total Pressure in Collector Chamber	5×10^{-4} torr
Peak Energy Flux Normal to Separatrix[c]	
Outer Plate	$2.5\ kW/cm^2$
Inner Plate	$1.1\ kW/cm^2$
Average Power Density on Inclined Target[c]	
Outer Plate	$0.2\ kW/cm^2$
Inner Plate	$0.13\ kW/cm^2$
Peak Power Density on Inclined Target[c]	$0.5\ kW/cm^2$
Peak Particle Flux on Inclined Target[c]	$1 \times 10^{18} cm^{-2} s^{-1}$
Total Active Area of Divertor Plates[c]	$57\ m^2$

[a] More recent assessments project 6.7 MW to outer divertor plate and 33 to inner divertor plate.

[b] On both sides of both separatrixes.

[c] Single null divertor.

11.5^{o} (0.2 radians) to reduce the heat and particle loads by a factor of 5 or more compared with those at normal incidence. For the inner divertor plate, the angle between the plate and the separatrix must be less than 26^{o} (0.46 radians) at the point where the plate crosses the separatrix. Since the inner branch of the divertor is blocked, the recommended arrangement is to build the divertor plate in two lobes converging on the separatrix at an angle less than 26^{o}, as shown in Figure 1. With this arrangement, the target would have to be fabricated carefully to assure there is a sharp inside corner between the lobes with no surface area normal to the separatrix.

Figure 1 also shows a continuous divertor plate intercepting both the inner and outer branch of the poloidal divertor. This configuration is recommended to simplify the coolant supply to the divertor plates and to ease removal and replacement of divertor plate assemblies as described in Section 1.1.4.

1.1.2 Coolant Selection

Basically, only three coolants have been considered in a fusion reactor, i.e., water, gases, and liquid metals. Gases and liquid metals can be eliminated due to poor heat transfer characteristics or MHD problems. Therefore, water is probably the only candidate for the coolant for the collector plate. Water can be used in the forced convection region, subcooled boiling region, or nucleate boiling region. A forced convection system is chosen for its good heat transfer characteristics at lower temperatures and to provide a larger safety factor on burn-out.

Water has been used to remove heat fluxes greater than 100 MW/m^2 (10 kW/cm^2) as indicated in Reference 1. Removal of such high heat fluxes requires high coolant velocity with swirl flow and large pressure

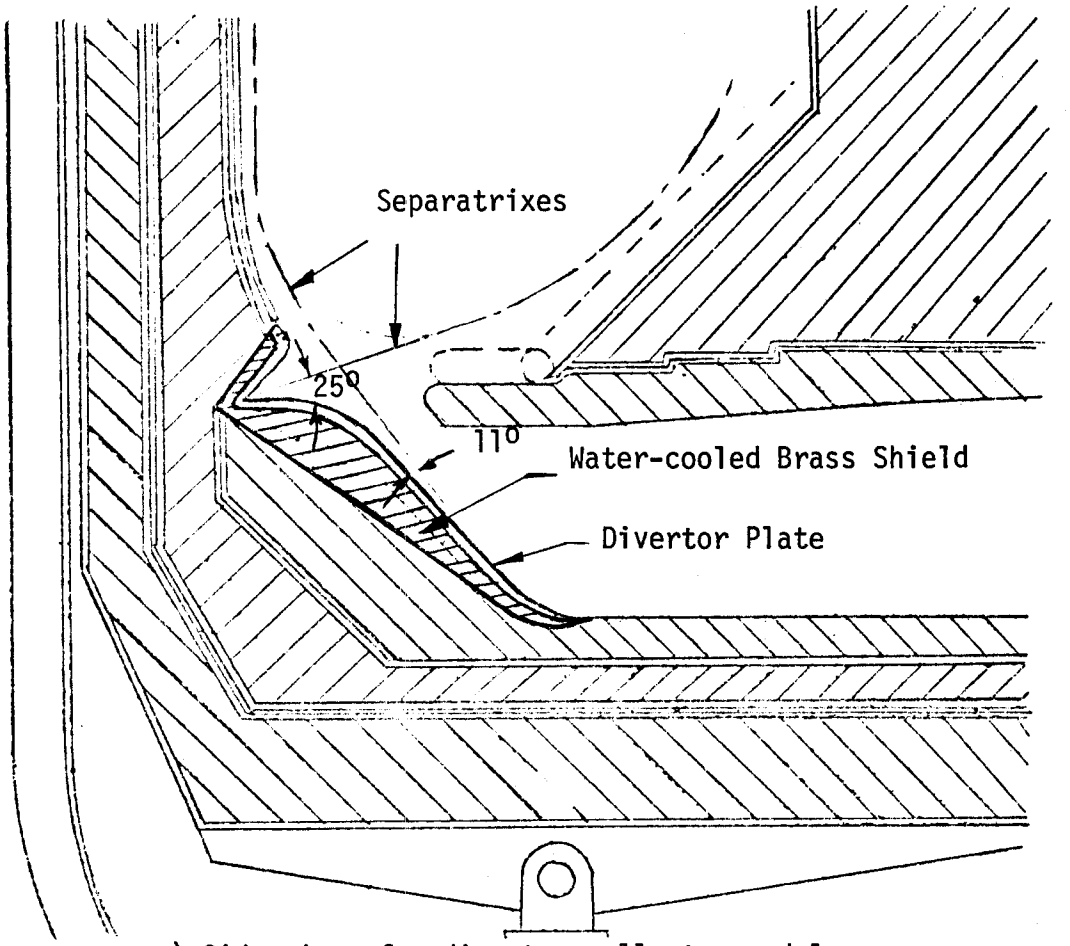

a) Side view of a divertor collector module.

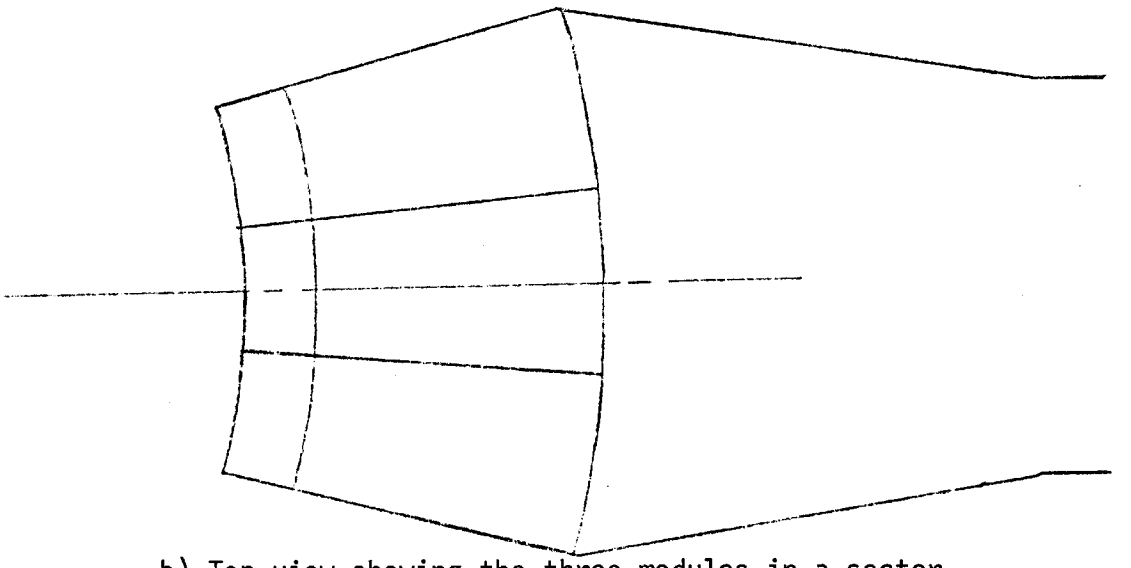

b) Top view showing the three modules in a sector.

Figure 1. Divertor collector module arrangement.

drops in the flowing liquid. For removal of 5 MW/m^2, on the other hand, relatively modest flow velocities, pressure drops, and coolant pressures are required as discussed for each design in Sections 1.2. and 1.3.

1.1.3. Coolant Structure Selection

The cooled structure of the divertor plate is subjected to a high heat flux. Therefore, thermal stress and temperature difference across the structure are the dominant factors in determining the structural material. Figure 2 shows the figure of merit for thermal stress of different materials as a function of temperature. It appears that copper, TZM and Ta-10 W are the most attractive ones. Copper is picked as the primary candidate for the structural material for its high thermal conductivity and fabricability. Ta-10 W is picked as the second choice for its good high temperature properties, low sputtering coefficient, and weldability.

1.1.4. Removal and Replacement

It is expected that there will be substantial uncertainties in the erosion rate of the selected divertor target through the design and fabrication stage. It is not likely that the lifetime of the divertor plate can be predicted accurately until actual operating experience is obtained in INTOR or a test module in TFTR or ETF. It is therefore important that the divertor plate be designed to allow for relatively easy replacement without a long delay in the operating schedule of the machine. The best approach for this appears to be to provide access for replacement through the divertor vacuum pumping duct while maintaining a vacuum in the plasma chamber. To accomplish this it will be necessary to develop a transfer cask that can be sealed to a vacuum flange on the divertor duct and evacuated.

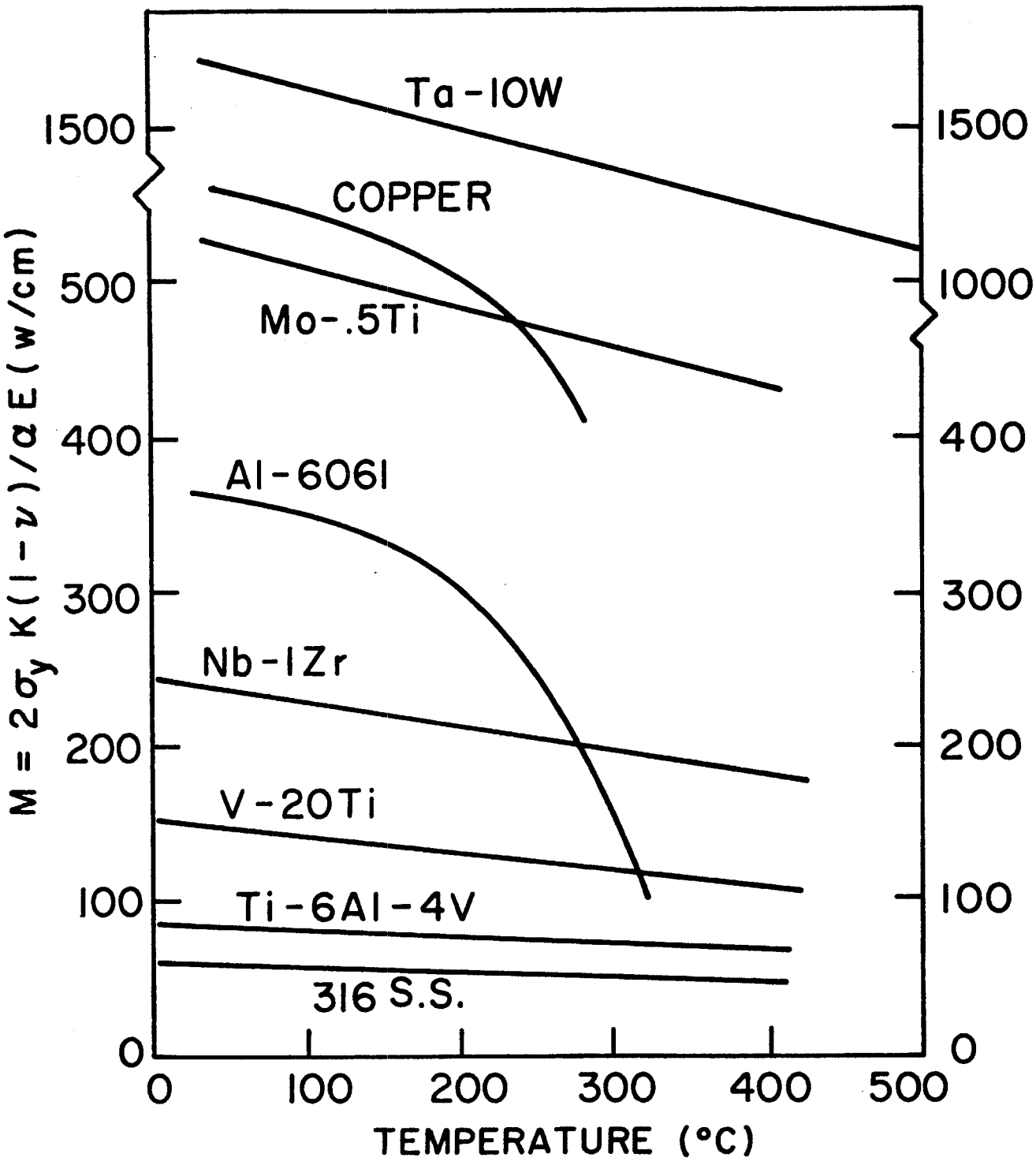

Figure 2. Thermal figure of merit as a function of temperature for several different structural alloys.

It is also necessary to modularize the divertor plate to provide for easy removal. This is done by combining the divertor plates for the inner and outer branches of the divertor into a single assembly. This combined structure is divided into three modules along radial planes (see Fig. 1) with the width of each module sized to allow it to be removed down the divertor vacuum duct. The center module in each sector is designed to be removed first and replaced last after the two outer modules have been placed in position. The center module serves to lock the two outer modules into position.

A track runs along the floor of the divertor duct and splits at a three way switch just before the divertor area. Each of the divertor modules is designed to be a two-wheel, single axle vehicle with a towing ball, as shown in Figure 3. The towing ball is offset toward the duct centerline on each of the two side vehicles. A creeper electric locomotive of about 4.5 tonnes tractive force can be sent via the three way switch to any of the vehicles. For removal, it proceeds to the appropriate station, lowers a socket and locks it onto the towing ball and lifts the ball to release the module. The module is then towed out to the shielded vacuum lock.

The wheel bearings on the divertor module are placed under the maximum thickness of the module to minimize radiation damage. Unlubricated ceramic-to-metal bearings are used. Should these bearings sieze or fail after irradiation in vacuum, it would be possible to drag the vehicle out on siezed wheels. The bearings are needed primarily for insertion of a new module, which must be driven up an inclined plane.

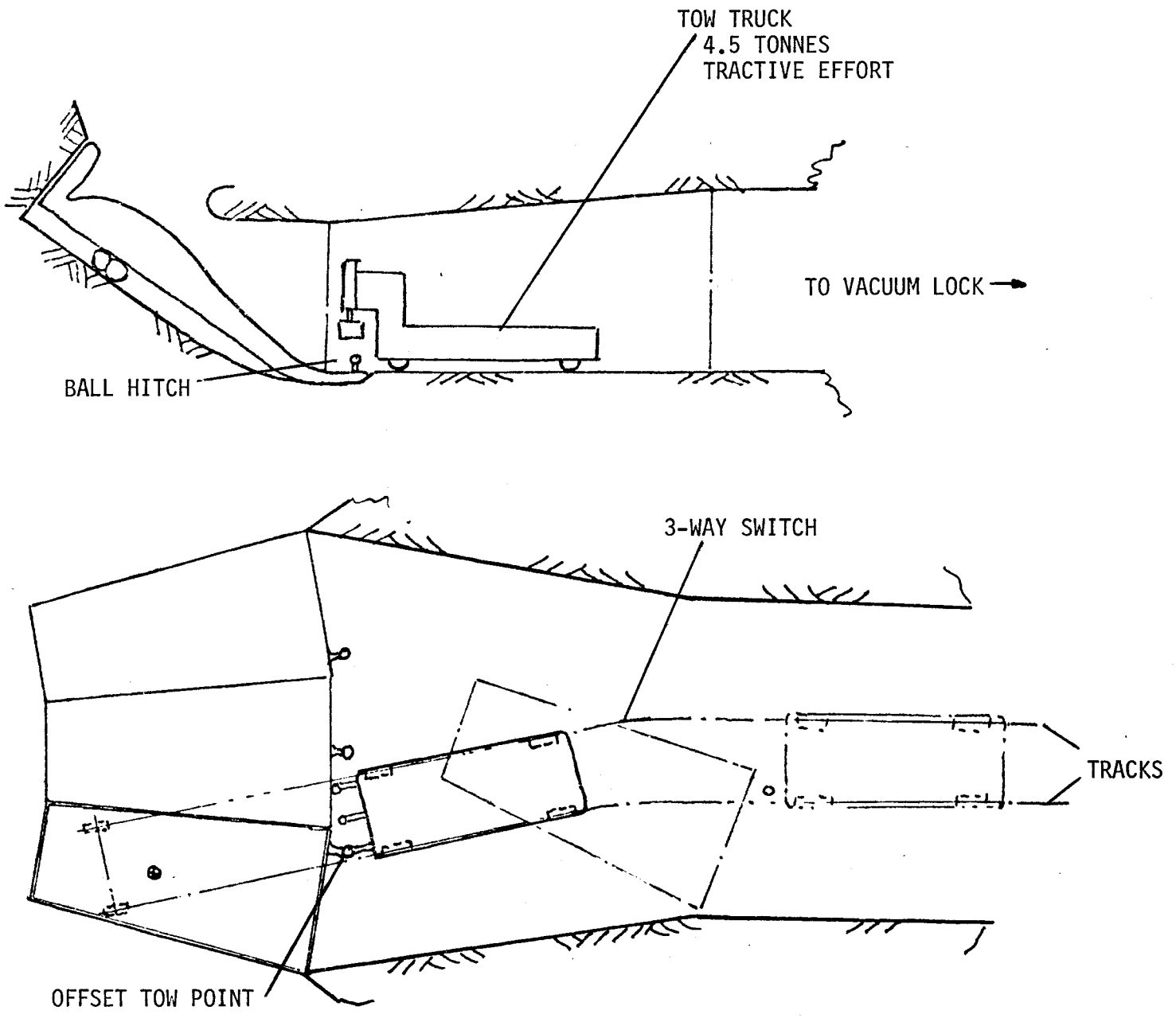

Figure 3. Divertor segment withdrawal.

The cooling water connections to the module are made directly to the underside of the divertor with a soft metal seal, as shown in Figure 4. The coolant pipe stretches downward about 4.5 m to an area where it is hand accessible, to make this joint.

The vacuum boundary is also carried to the same area by a surrounding tube and sealed to the water pipe with a polymer seal, permitting rotation of the water pipe to make and break the joint with the divertor module. This polymer seal only holds the vacuum during pipe connecting operations. When these are complete, a welded joint is made. The pipe will be loosely guided by the vacuum tube during connecting and disconnecting and a generous lead will be provided to guide the top of the pipe into the prepared tapped and faced orifice in the underside of the divertor. The vacuum extension pipe may be detached from the shield to allow major sector removal. During sector removal the water pipe must be dropped completely clear, if necessary, into a well in the floor. Two pipes, an inlet and an outlet, are connected to each module.

1.2. RECOMMENDED DESIGN - SOLID TARGET

In the solid target design, tungsten tiles 1 cm thick are placed between the water-cooled copper heat sink and the plasma. These tiles are bonded to the copper and serve as armor to protect the copper from erosion by charged particles and energetic neutrals.

1.2.1. Material Selection

The most critical property of the material on which the plasma stream impinges is the sputtering yield. The sputtering yield determines the lifetime of a plate of given thickness or determines the initial thickness required to reach the desired lifetime. The thermal

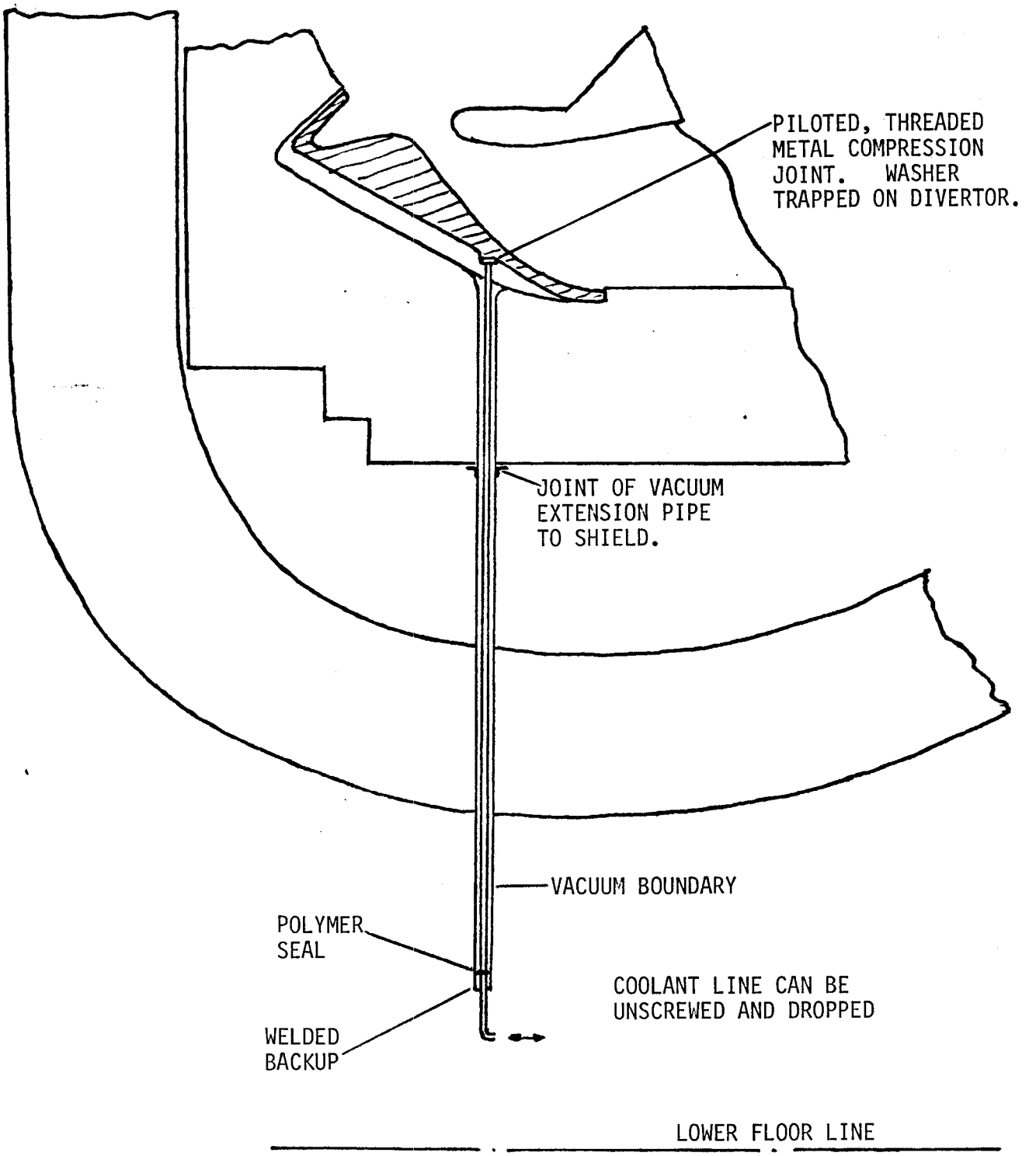

Figure 4. Divertor segment coolant connection.

conductivity of the material is also an important property which affects the temperature difference developed across the material during operation.

The properties of several materials are compared in Table 2. As shown here, tungsten is clearly the best choice because of its low sputtering yield and high thermal conductivity. The nearest contender to tungsten is CSCA, which is not currently available in the thickness required. ATJ-S graphite and silicon carbide are also attractive materials, but require relatively large thicknesses with large temperature differentials and high thermal stresses.

Two drawbacks that have been noted for tungsten are that it is a high Z material and that it is brittle and relatively difficult to fabricate. It appears that the fabrication difficulties can be overcome by several means. Tungsten tiles or large tungsten plates formed by powder metallurgy techniques can be brazed to copper by several techniques that are within the state-of-the-art. Tungsten may also be formed in the required shapes by chemical vapor deposition by hydrogen reduction of WF_6. This may be the cheapest method of fabricating tungsten for this application. Although tungsten is brittle at room temperature, thermal stresses in the tungsten should be generally low due to the high thermal conductivity and low thermal expansivity of this material. Furthermore, local cracks which may form in the tungsten armor should not propagate into the ductile copper substrate that provides the containment for the water coolant. Should it prove desirable to seek a ductile metal for the armor, tantalum is a viable candidate as may be seen in Table 2.

Although plasma contamination due to sputtered impurities is likely to disqualify a high Z material like tungsten as a first wall material,

Table 2. Evaluation of Candidate Materials for INTOR Divertor Plate Armor

Material	Sputtering Yield[e] (#/ion) (@ 1 keV, D+)	Thermal Conductivity (W/m°K)	Erosion Rate[f] (mm/yr) -x-	ΔT (°C) Across Thickness x	Melting Point (°C)
ATJ-S[a]	1.7×10^{-2}	55	10.5	955	3500[c]
CSCA[b]	10^{-3}	10	.62	308	
SiC	3×10^{-2}	55	16.8	1530	2600[d]
Cu	1×10^{-1}	391	65.	832	1083
SS	2.9×10^{-2}	16.3	18.6	5710	2550
Mo	6.3×10^{-3}	146.2	5.5	187	2610
INC-718	3.7×10^{-2}	11.2	22.5	10000	2400
Ta	1.6×10^{-3}	54.5	1.6	148	2996
Ti	1×10^{-2}	10	9.7	4860	1668
W	8.7×10^{-4}	167	.8	24	3380

[a] ATJ-S "UCAR" Graphite Grade ATJ-S.

[b] A carbon-silicon carbide alloy (94% carbon, nominal 6% SiC), General Atomic- applied as a coating.

[c] Vapor Pressure = 1 atm.

[d] Decomposition to element.

[e] Atomic Data for Controlled Fusion Research, ORNL-5207.

[f] At 25% Availability and 70% Duty Factor.

this may not be a serious problem for a divertor plate. Pumping by the plasma stream may return almost all of the sputtered tungsten to the divertor plate or the divertor vacuum duct and limit plasma contamination to acceptable levels (Ref. 2). In any event, our present knowledge of plasma interaction with divertor plates provides no basis to disqualify tungsten as a divertor armor plate material. Should plasma contamination by tungsten prove to be unacceptable, graphite and silicon carbide are potential alternate materials. Should either be used, it would probably be necessary to accept a shorter lifetime for the divertor plate in order to limit thermal stresses in these materials to acceptable levels.

Recent preliminary calculations of divertor channel modelling have indicated the potential for sputtering by charge exchange neutrals from the section of the collector between the separatrixes. A significant fraction of the atoms sputtered from this region might enter the plasma, since there are no channel walls facing the plate at this point (See Fig. 1). Should the resulting plasma contamination with tungsten be excessive, it should be possible to reduce contamination by reconfiguring the channel. In addition, a low-Z material like graphite or SiC might be used in the region of the plate from which sputtered atoms are more accessible to the plasma. Since particle fluxes are low in this region, a relatively thin armor layer could be used without shortening the sputtering erosion life below 2 years.

1.2.2. System Description and Configuration

The reference design for the divertor plate consists of tungsten tiles 2 x 2 cm square and 1 cm thick that are brazed to a 1.2-cm thick copper plate that has internal cooling passages (see Fig. 5). The major parameters of the reference design are summarized in Table 3.

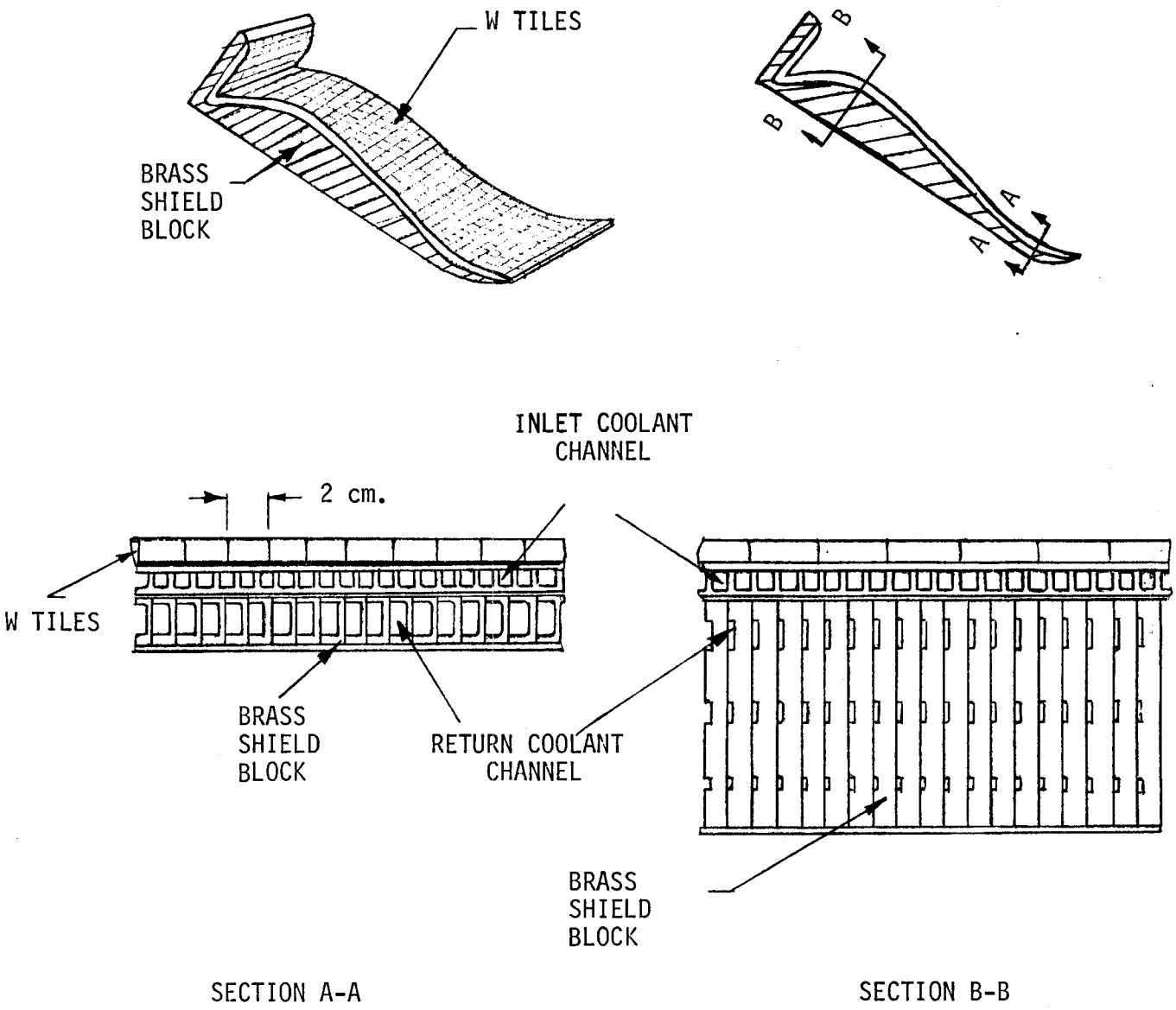

Figure 5. Divertor plate module.

Table 3. Design Parameters of Solid Divertor Plate

Armor Material	W
Thickness of Armor	10 mm
Heat Sink Material	Cu
Thickness of Heat Sink	10-12 mm
Width of Coolant Channels	5-7 mm
Depth of Coolant Channels	5-7 mm
Flow Velocity in Coolant Channels	7.5 m/s
Heat Transfer Coefficient	4 W/cm^2 K
Coolant Inlet Temperature	40°C
Coolant Outlet Temperature	65°C
Coolant Volume Flow Rate	1 m^3/s
Coolant Inlet Pressure	0.79 MPa
Coolant Pressure Drop	130 kPa
Coolant Pumping Power	130 kW
Peak Film Temperature Drop	127°C
Peak Wall Temperature	190°C
Peak Braze Temperature	240°C
Peak Tungsten Temperature	370°C

Coolant flow enters the outer divertor plate at its outer edge and is distributed through a manifold into many small parallel passages. The coolant flows through these passages towards the centerpost of the machine removing heat first from the outer and then from the inner branch of the divertor and returns through a section of shielding below the divertor plate. The shielding through which the water returns is an integral part of the divertor plate module. The section of shielding is incorporated in the module in order to allow sufficient clearance for removal of the divertor plate modules through the vacuum duct as described in Section 1.1. This removable shield is made of brass, which can be easily joined to copper to make a reliable leak-tight coolant circuit. The removable water cooled shielding is expected to attenuate neutrons and gamma radiation about as well as the stainless steel below it.

The radial flow direction was selected to make the heat removed by the water in each parallel channel as nearly equal as possible regardless of the exact location of the separatrixes. This flow arrangement, however, requires the channels to have a variable width, since the width of the divertor plate is reduced by nearly a third between the outside of the outer plate and the innermost point of the inner plate. The width of the coolant channels is reduced from about 7 mm at the outer radius to about 5 mm at the inner radius, while the depth of the channels is increased from about 5 mm at the outer radius to 7 mm at the inner radius to maintain the flow in the channels at about the same 7.5 m/s velocity. This arrangement is shown in Figure 6. The tungsten tiles

are joined to the copper heat sink by means of a copper-silver braze alloy, AWS BAg-8. The braze is applied by first plating a thin layer of nickel ($\sim$2 μm) on both the tungsten and copper. The nickel is used to serve as a diffusion barrier. The braze is then made at 780°C in a vacuum or hydrogen atmosphere.

The BAg-8 braze alloy is expected to have an extremely high thermal conductivity, which is important for this high heat flux application. Its electrical conductivity is reported to be 89% of that of the International Annealed Copper Standard. This is a well established braze system with which there is considerable industrial experience in joining copper to tungsten heater wire.

1.2.3. Estimated Lifetime

The erosion rate of tungsten was calculated from revised sputtering yields (Ref. 3) for a mixture of deuterium, tritium and helium with a Maxwellian energy distribution about 1.35 keV. The erosion rate calculated was found to be substantially higher than that shown in Table 2, which was based on an older data source. The calculated erosion rate of 4.9 mm/yr indicates that the tungsten armor would have a lifetime of 2 years in the INTOR machine operating at its specified availability.

Erosion is the major mechanism for failure of the divertor collector plates. There is also the possibility, however, that thermal fatigue due to the bimetallic joint between copper and tungsten could lead to premature failure of the copper heat sink or the bond between the two metals. It was concluded that this question can only be resolved definitively by an experimental program.

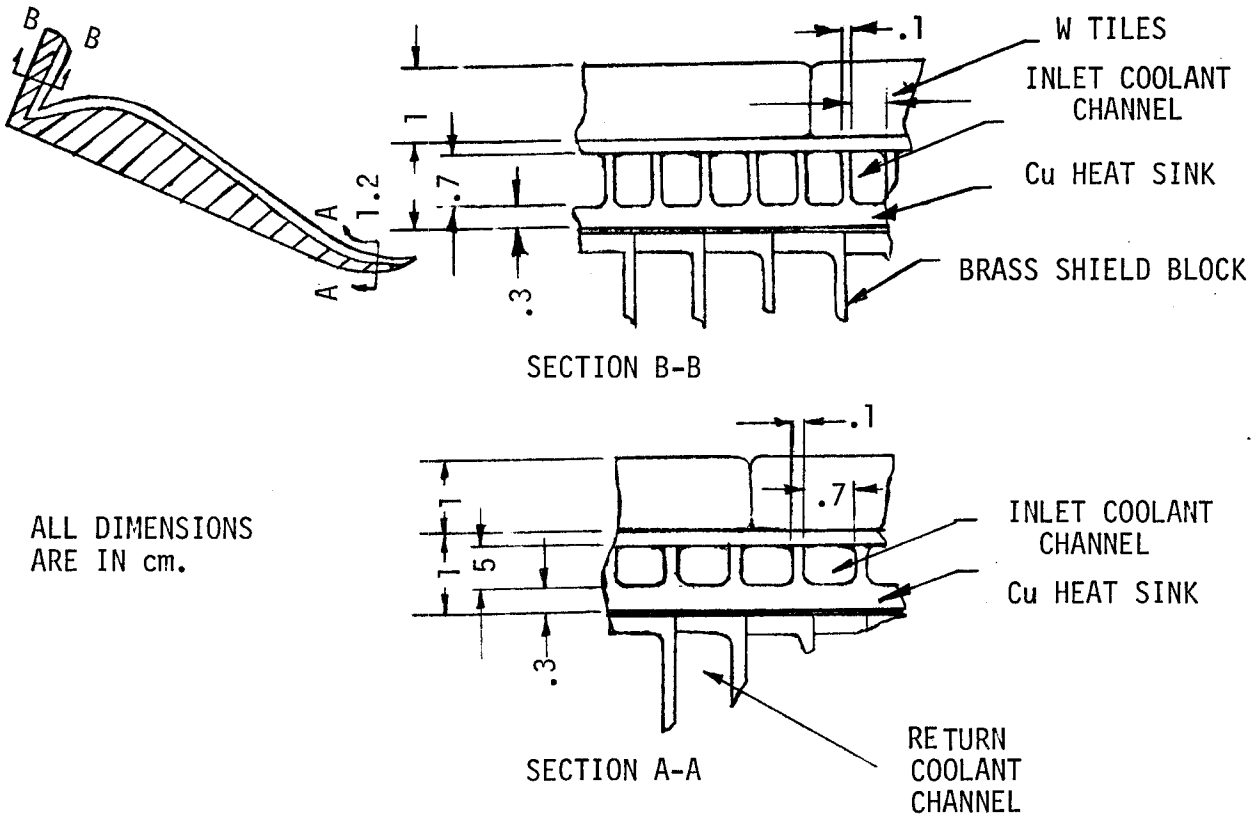

Figure 6. Coolant channels at large and small poloidal radii.

1.2.4 Estimated Cost

In order to evalute the economic impact of the divertor plates, a cost estimate of the reference design was made, based on unit costs of fabricated materials given in Reference 4. The divertor collector is divided into 36 modules. The materials are tungsten, copper and brass for the armor, heat sink and shielding regions, respectively, of the divertor plate modules as shown in Figure 5. Table 4 summarizes the input data and results of this cost estimate. The unit cost data of copper was used instead of brass for the shielding region because of the limited available cost data. It is expected that the unit cost for brass would be slightly less than that for copper.

The material volumes were estimated by using a total plate area of 74 m^2 and thicknesses for the tungsten, copper and brass regions of 1 cm, 1.2 cm and 20 cm, respectively.

Table 4. Cost Estimate of Divertor Plates

Material	Unit Cost ($/kg)	Volume (m^3)	Mass (kg)	Cost in $ 10^6
Tungsten	80[a]	.74	14282	1.14
Copper	20[b]	.485	4365	0.09
Brass	15[c]	14.05	126450	1.90
Total			1.45×10^5	3.13
Number of Modules		36		
Mass per Module		4030 kg		
Cost per Module		$86,860		

[a] Plates sintered from powder

[b] Complex machinery

[c] Copper stamped for cooling

As can be noted from Table 4, the dominant mass is that of the brass shield because of its large volume. Even though the tungsten plates have a relatively small total volume, their cost is quite high because of the high unit cost of tungsten. The total cost of the divertor plate modules, however, appears to be no more than twice the cost of an equivalent volume of stainless steel shielding.

1.3. RECOMMENDED DESIGN - LIQUID TARGET

1.3.1. Material Selection

There are two critical problems associated with the thermal-mechanical design of the divertor plate, i.e., sputtering and heat transfer. The liquid target concept is desirable on sputtering considerations, since the liquid film can easily be reestablished. However, there are difficult heat transfer and vaporization problems. The concept developed here is to use a liquid film for sputtering protection, while a forced convection loop is used for heat removal.

The ideal liquid target material would have the following properties:

1. Low Z
2. Low vapor pressure
3. Low sputtering coefficient
4. High stability
5. Low melting temperature
6. High thermal conductivity.

Natural lithium appears to satisfy most of the requirements and is, therefore, picked as the target material.

1.3.2. System Description and Configuration

A schematic view of the proposed system is shown on Figure 7. The particles from the plasma impinge on a layer of lithium 0.5 mm thick. The lithium film is formed by either a flow of falling film, or by spraying during the plasma down time. The lithium film covers a copper plate 3 mm thick. The thermal energy is transferred by conduction through the lithium film and the copper plate and is carried away by a stream of high velocity water. Such a design decouples the solution to the sputtering and heat transfer problems.

To simplify the coolant supply systems and collector removal scheme, a single structural configuration for both inside and outside collector plates, as suggested previously and shown on Figure 1, is highly desirable. The coolant supply system is schematically shown on Figure 8. Each coolant tube will be subjected to a different thermal load, and a flow resistance will be built into the coolant tubes with a low thermal load.

The thermal hydraulics parameters of the collector plate are listed on Table 5.

1.3.3. Estimated Lifetime

The lifetime of the divertor collector plate can be limited by either sputtering, fatigue or radiation damage. The fatigue and radiation damage problems have not been considered in this study. However, they are not expected to be the life limiting factor due to the low stress (60 MPa) and the low structure temperature (<.4 x melting temperature).

If the design of the wetted wall is ideal, sputtering will cause no erosion on the structure. However, dry spots may occur on the plate,

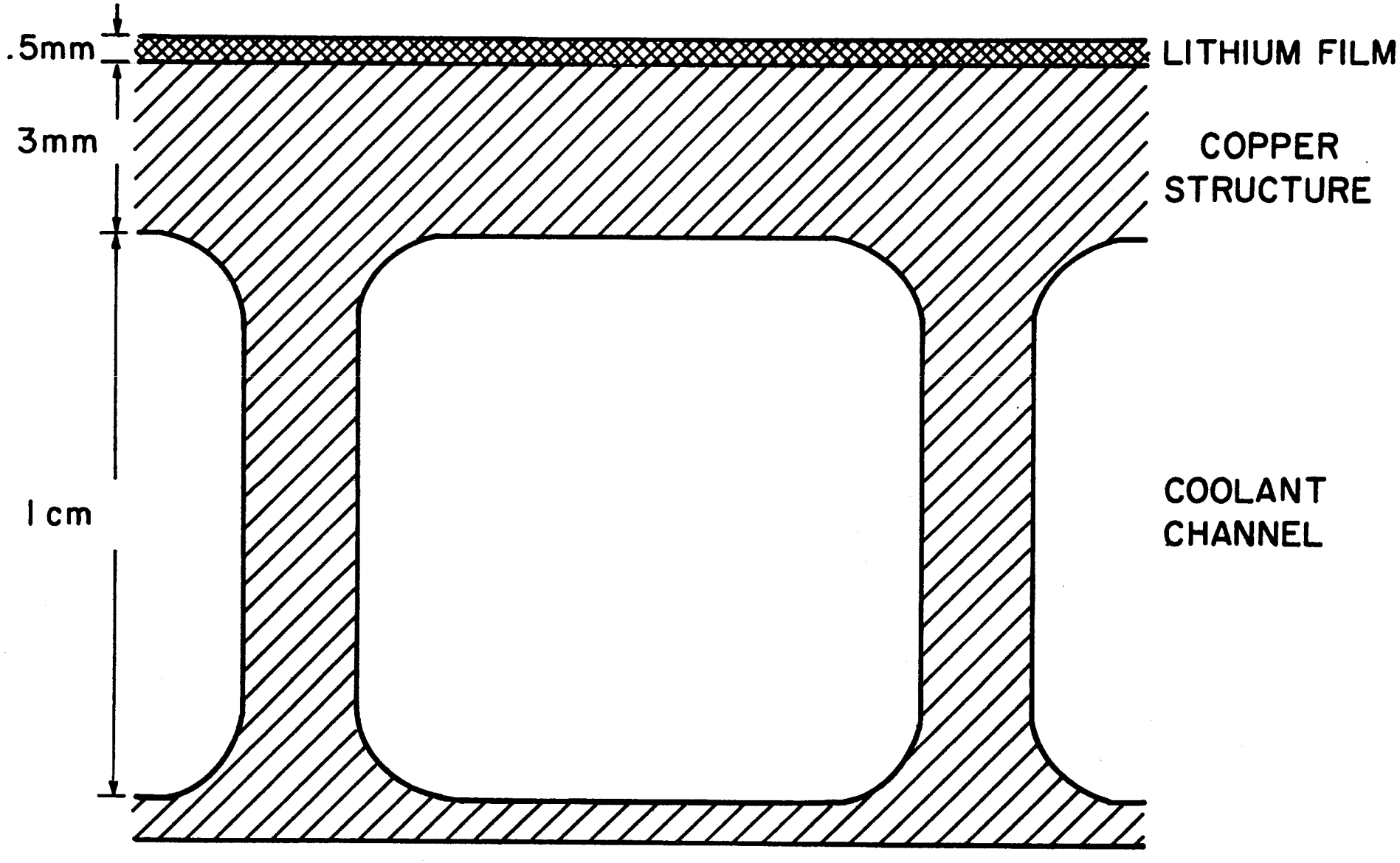

Figure 7. Cross-sectional view of wetted wall divertor plate design

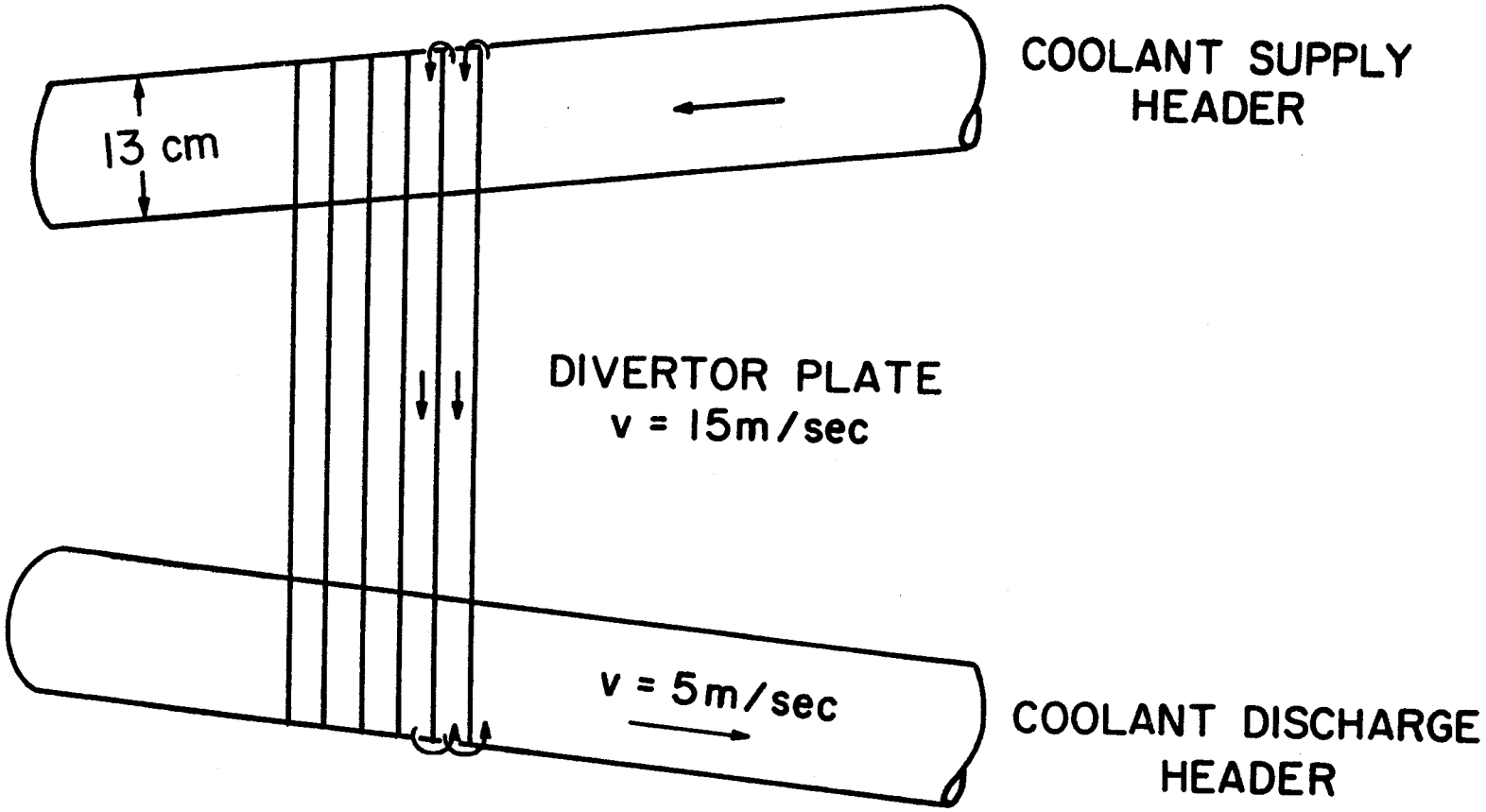

Figure 8. Coolant supply system for divertor plate

Table 5. Thermal hydraulic parameters of a wetted wall divertor plate.

Wall protection	Li
Liquid film thickness	0.5 mm
Percent area of divertor plate covered	90%
Plate structure	Copper (Ta-10 W)
Plate thickness	3 mm
Coolant tube ID	1 cm
Coolant	Water
Coolant velocity	15 m/sec
Coolant heat transfer coefficient	5 W/cm^2-^oC
Maximum thermal load	500 W/cm^2
Coolant inlet temperature	100^oC
Coolant outlet temperature	110^oC
Coolant flow rate	2400 kg/sec
Maximum structure temperature	250^oC
Maximum lithium temperature	310^oC
Lithium vapor pressure	10^{-6} torr
Lithium sputtering rate	$4.5 \times 10^{21} sec^{-1}$
Lithium evaporation rate	$2 \times 10^{20} sec^{-1}$
Lithium flow rate to plasma chamber	$2.1 \times 10^{21} sec^{-1}$

either due to a non-ideal liquid film or the non-wetting of the solid surface by the liquid.[a] If 95% coverage can be assumed and a sputtering coefficient of .1 is used, a wall life of six months will be expected.

The trajectory of the particle incident on the collector plate will be of major importance to the sputtering. If the incident angle θ, as shown on Figure 9, is small, there will be excellent protection of the plate if a small dry spot occurs. The six month wall lifetime did not take this effect into consideration and is, therefore, conservative.

1.4. ALTERNATIVE DESIGNS

A few alternative designs have been studied briefly. The first three described below are variations on the reference solid target divertor plate design. The last one is a completely different concept.

1.4.1. Use of a Tantalum Heat Sink With Tungsten Armor

The possibility of using tantalum instead of copper for the heat sink was investigated as a means to reduce stresses due to the mismatch in thermal expansion between copper and tungsten. Although the temperature at the joint between tungsten and tantalum would be much higher (750°C vs. 250°C for the copper-tungsten joint), the stress was found to be less because of the good match in thermal expansion between tungsten and tantalum. More important, the yield strength of tantalum is substantially greater than that of copper and is nearly equal to the thermal stress indicating that there will be no yielding beyond the first thermal cycle. Tantalum appears to be an acceptable alternative to copper if the tungsten-copper system proves to be unable to endure thermal cycling. The difficulties of fabricating complex structures of tantalum, however, would have to be overcome.

---

[a] D. Kummer of McDonnell-Douglas has suggested the use of a fine wire net to cover the surface, by capillary action, would insure uniform distribution of the liquid Li. This may mitigate the concern over "dry spots".

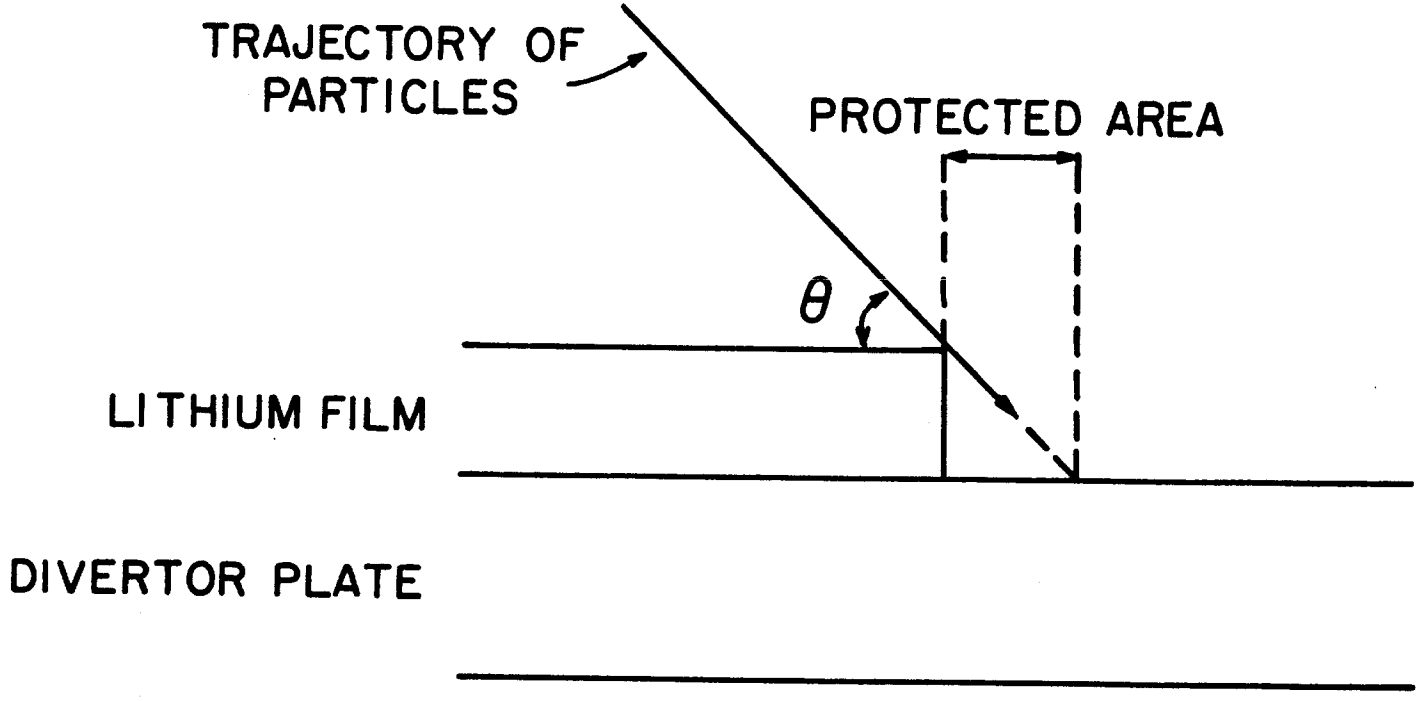

Figure 9. Effect of incident angle to wall protection

1.4.2. Use of Tantalum as Armor

The possibility of using tantalum as the armor was investigated, because tantalum is a ductile metal that has superior thermal stress resistance and is easier to fabricate than tungsten. Table 6 compares the pertinent parameters for material selection between tungsten and tantalum.

Table 6. Comparison of Tungsten and Tantalum as Armor

	Tungsten	Tantalum
Density (kg/m^3)	19300	16600
Melting Point (^oC)	3410	2996
Thermal Conductivity (W/m K)	167	54.5
Sputtering Yield E = 1.34 keV, D+ (atoms/ion)	3.9×10^{-3} (Ref. 3)	8.5×10^{-3} (Ref. 5)
Erosion Rate, x (mm/yr)	4.9	12.2
ΔT Across x, @ 5 MW/m^2 (^oC)	147	1119
Relative Armor Cost	1	9

From Table 6, one can see that the erosion rate of tantalum is higher, the temperature difference across the armor is greater, and a plate that can last for the same lifetime is thicker and is much more expensive than tungsten. Tantalum would only be used for divertor plate armor if thermal stress failure, fabrication difficulties or other problems make it impossible to use tungsten.

1.4.3. Low Z Armor Materials

Low Z materials were considered as alternate armor materials for the divertor plates to reduce the effects of plasma contamination.

From Table 2 it may be seen that ATJ-S graphite and SiC are possible candidates because of their high temperature capabilities, relatively high thermal conductivities and acceptable erosion rates.

ATJ-S graphite can possibly be attached to the copper plate by graphite cement. A more reliable method is by mechanical attachment, using graphite screws to hold the graphite plates onto the copper plate. With this form of attachment, graphite cement would still be needed to enhance heat transfer between the graphite and copper plates. More details of this attachment method will need to be investigated if this approach is chosen for further study.

SiC can be attached to copper by first depositing a thin ($\sim$25 μm) layer of tungsten onto SiC by chemical vapor deposition or ion plating and then brazing the tungsten coated surface to copper by the same method as specified for joining tungsten to copper for the reference design (Section 1.2.2.).

Graphite is easier to machine and less expensive than SiC, but SiC would be less susceptible to neutron irradiation damage.

The sputtering yield of these materials is sensitive to temperature, energy of the charged particles, and also the method of manufacturing. The thermal conductivities of these materials also vary greatly with temperature (e.g., from $\sim$70 W/m^{o}K at 500^{o}C to 40 W/m^{o}K at 1200^{o}C, for ATJ-S). Since both of these properties are crucial to armor plate performance, the effects of the operating environment and manufacturing technique will have to be considered carefully should low Z armor material be selected for further study or development.

Table 7 gives comparative cost estimates for armor materials ATJ-S, SiC and W. The mass per module includes the copper heat sink

and shielding material behind the divertor plate. The armor plates compared in this section have thicknesses required for a lifetime of ∿1 year, whereas the reference W design has a lifetime of ∿2 years.

Table 7. Cost Comparison of ATJ-S, SiC and W

Material	Thickness[a] (cm)	Volume (m^3)	Mass/Module[b] (kg)	Total Cost[b] $ 10^6
W	0.5	.37	3832	2.56
ATJ-S	1.5	1.11	3702	2.05[c]
SiC	2.5	1.78	3791	3.48[d]

[a]Thicknesses required for ∿1 year of operation.

[b]Mass/module and total cost include armor plates, copper heat sink and brass shield.

[c]Unit cost of graphite $25/kg for plain liner, thin squares 1 cm thick.

[d]Unit cost of SiC, $265/kg for coating and liner.

The mass/module are similar for these materials because their masses are dominated by the 20-cm thick brass shield. SiC is the most expensive because of the required thickness and the higher unit cost. It is concluded that both ATJ-S and SiC are viable armor materials for the divertor plates when the use of low Z material is a requirement, yet they may have a shorter lifetime than W.

1.4.4. Multiple Channel Divertor Plate Concept

An alternative design has been suggested (Ref. 6) and is shown schematically on Figure 10. The structural material is aluminum and the coolant is forced convection water. The basic idea is to provide multiple layers of coolant channels so that, after the first layer is sputtered away, the coolant will be switched to the second row of coolant tubes. However, as shown on Figure 2, aluminum has a low value of figure of merit of thermal stress. To keep the thermal stress under 100 MPa, a maximum wall thickness of only 2 mm can be allowed, which translates to a two week lifetime for each layer.

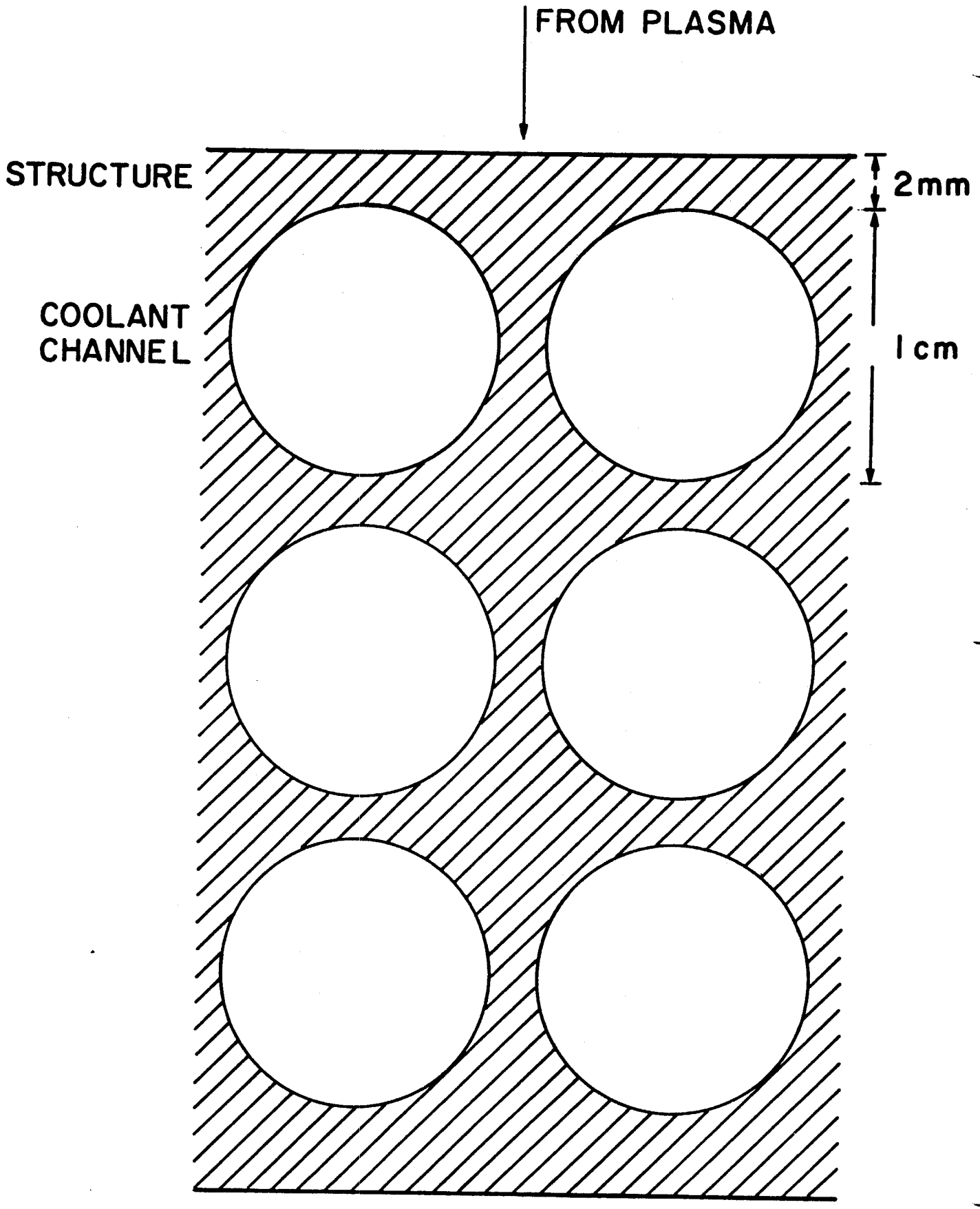

Figure 10. Multiple channel divertor plate concept.

2. SUPPORTING INFORMATION AND ANALYSIS

2.1. SOLID TARGET

2.1.1. Stress Analysis of the Tungsten-Copper Joint

A preliminary stress analysis was made to estimate the effects of the large strain differences that would be generated at the discontinuity between tungsten and copper as a result of the mismatch in their thermal expansivities. The stresses in copper calculated by elastic analysis are far beyond the yield stress and indicate that the copper will be forced to yield during each thermal cycle between room temperature and the peak operating temperature. The ductility of copper combined with the partial annealing that would be produced at the peak operating temperature of 250°C indicate that repeated yielding may not create a serious problem limiting lifetime. The only reliable way to determine whether the thermal cycling will lead to problems is to design and fabricate appropriate test specimens and subject them to a thermal cycle test.

2.1.2. Effects of Radiation on the Copper Heat Sink

The maximum operating temperature of the copper heat sink is expected to be 250°C. At this temperature and a fluence (>0.1 MeV) of about 5×10^{21} n/cm^2 (∿5 dpa), copper swelling should be small. Extrapolation of 0.5 dpa fission data (Ref. 7) gives an estimated maximum swelling of <1% for copper at 250°C (0.39 T_{mp}[a]) and 5 dpa. The swelling peak in copper is at about 350°C (0.44 T_{mp}). The possible additional effects of the 33 appm of transmutation produced He on swelling cannot be estimated at this time.

---

[a] T_{mp} = melting point temperature on the absolute scale.

At the 40-250°C operating temperature of the heat sink, copper will decrease in ductility due to displacement damage. The magnitude of this change is difficult to predict for divertor target neutron spectra and fluences, but existing fission spectrum data on annealed copper (ductility 27-34%) indicate a decrease in ductility to approximately the value for unirradiated 60% cold worked material (17%) after exposure to less than 10^{20} n/cm^2 (Ref. 8). Reduction of ductility, which is a measure of the ability of a material to relieve local stress concentrations without fracturing, to values below a few percent would be a major concern in the copper heat sink which is subjected to cyclic thermal loads during service. At 250°C, the mobility of He in copper is too low to significantly embrittle the material by the conventional grain boundary bubble formation mechanism. However, the 33 appm He produced from (n,α) reactions could contribute to increased matrix stiffening by refining the irradiation produced defect structure.

2.2 LIQUID TARGET

2.2.1. Temperature Calculations:

Coolant velocity = 15 m/sec

Coolant channel I.D. = 1 cm

$Re = Dv\rho/\mu = 10^6$

Heat transfer coefficient = $h = \frac{K}{D} \times 0.023\ (Re)^{0.8}\ (Pr)^{0.4}$

$= 5\ W/cm^2\text{-}^oC$

Film temperature drop = $Q/h = 100^oC$

Tube wall thickness = 3 mm

$K]_{copper} = 3.91\ W/cm\text{-}^oK$

$\Delta T]_{\text{tube wall}} = Qx/K = 38^{o}C$

Thermal stress $= \frac{\alpha E}{2(1-\nu)} \Delta T$

For copper $\alpha = 18 \times 10^{-6}/^{o}C$

$E = 17 \times 10^{6}$ psi

$\nu = .3$

$\sigma_{Th} = 57.3$ MPa

Lithium film thickness = .5 mm

$K]_{Li} = .42$ W/cm-^{o}K

$\Delta T]_{Li}$ film $= 60^{o}C$

2.2.2. Sputtering and Evaporation Calculations

Maxwellian sputtering coefficients for divertor plate materials were calculated by Smith (Ref. 3) and are shown on Table 8. The sputtering coefficients for lithium are estimated to be 0.0182 and .0272 for D and T, respectively. The total loss rate of lithium atoms due to sputtering is calculated to be 4.5×10^{21}/sec. Sputtering and evaporation calculations for lithium are summarized in Table 9.

Acknowledgement

Funding in part has been provided by the U.S. Department of Energy.

Table 8. Maxwellian Sputtering Coefficients for Divertor Plate Materials (Ref. 3)

	Energy-eV					
	1350			500		
	D	T	He	D	T	He
C	0.0090	0.0135	0.0435	0.0113	0.0170	0.0442
W	0.0039	0.0063	0.0120	0.0015	0.0028	0.0049
Al	0.0231	0.0346	0.0950	0.0227	0.0343	0.0749
Li[a]	0.0182	0.0272				

[a]Sputtering coefficient for Li is for monoenergetic particle at 1350 eV.

Table 9. Summary of Lithium Sputtering and Evaporation Calculations

	Inner	Outer
Total Energy	25 MW	75 MW
Maximum Q	500 W/cm^2	500 W/cm^2
Total Particles	5×10^{22}/sec	1.5×10^{23}/sec
Sputtering Coefficient	.0227	.0227
Sputtered Particle	1.1×10^{21}/sec	3.4×10^{21}/sec
Temperature	310	310
P_{Li}	10^{-6} torr	10^{-6} torr
v_{Li}	1.33×10^5 cm/sec	1.33×10^5 cm/sec
ρ_{Li} (at 10^{-5} torr)	1.55×10^{10} #/cm^3	1.55×10^{10} #/cm^3
A (Q/500 W/cm^2)	5×10^4 cm^2	1.5×10^5 cm^2
$A\rho v/2$	5×10^{19} #/sec	1.5×10^{20} #/sec
Total Particles	1.15×10^{21} #/sec	3.55×10^{21} #/sec
Fraction Returned to Plasma Chamber	1	0.25
Particle Returned to Plasma Chamber	1.15×10^{21} #/sec	$.88 \times 10^{21}$ #/sec
# of lithium of plasma chamber	2.1×10^{21} #/sec	

REFERENCES

1. GAMBILL, W. R. and N. D. Greene, "Boiling Burnout with Water in Vortex Flow", Chem. Eng. Prog. 54:68 (1958).

2. SCHMIDT, J. A., Princeton Plasma Physics Laboratory, Personal Communication.

3. SMITH, D. L., Argonne National Laboratory, Personal Communication, based on paper in "Proceedings of Workshop on Sputtering Caused by Plasma-Surface Interaction", July 1979, CONF-790775.

4. SCHULTE, S. C., et al., "Fusion Reactor Design Studies, Standard Cost Estimating Rules", PNL-2987, Pacific Northwest Laboratory, September 1979.

5. MEYER, C. H., J. N. Smith, Jr., "H+ and D+ Sputtering of Thin Tantalum Films in the Energy Range of 0.6 to 15 keV", J. Vac. Sci. Technol., p. 248, 16(2), Mar./Apr. 1979.

6. FILLO, J., Brookhaven National Laboratory, Personal Communication.

7. ADDA, Y., "Report on the CEA Program of Investigations of Radiation-Induced Cavities in Metals: Presentation of Some Results," Radiation Induced Voids in Metals, J. W. Corbett and L. C. Iannsello, Eds., U. S. AEC, April 1972, pp. 75-77.

8. "GAC-ANL TNS Scoping Studies, Status Report for FY77, October 1, 1976 - September 30, 1977, Volume V, Support Engineering, Tritium and Neutronics," Argonne National Laboratory, Report No. GA-A14614, January 1978.